Geochimica et Cosmochimica Acta 355 (2023) 1–12

Contents lists available at ScienceDirect

Geochimica et Cosmochimica Acta

journal homepage: www.elsevier.com/locate/gca

Redox and mineral controls on Fe and Ti isotopic fractionations during calc-alkaline magmatic differentiation

Aleisha C. Johnson [a,b,*], Zhe J. Zhang [a], Nicolas Dauphas [a], Roberta L. Rudnick [c], John D. Foden [d], Magali Toc [c]

[a] Origins Laboratory, Department of the Geophysical Sciences, The University of Chicago, Chicago, IL, USA
[b] Department of Geosciences, University of Arizona, Tucson, AZ, USA
[c] Department of Earth Science and Earth Research Institute, University of California – Santa Barbara, Santa Barbara, CA 93105, USA
[d] Department of Geology, University of Adelaide, Adelaide, SA, Australia

ARTICLE INFO

Associate editor: Sheng-Ao Liu

Keywords:
Titanium isotopes
Iron isotopes
Magmatic differentiation
Calc-alkaline magma series

ABSTRACT

Titanium and Fe isotopic compositions of lavas from a calc-alkaline differentiation suite and corresponding mineral separates from the Rindjani Volcano, Indonesia show that Fe and Ti isotopic fractionations between minerals and melts are lower than those recorded in other suites at all stages of differentiation. The limited isotopic fractionation for Ti is likely due to low-Ti magnetite and clinopyroxene being the dominant carriers of Ti in Rindjani lavas, as these minerals are thought to have limited equilibrium Ti isotopic fractionation relative to silicate magmas. Other magmatic differentiation suites controlled by removal of Ti-rich magnetite and characterized by a lesser role of clinopyroxene have larger Ti isotopic fractionations. This effect is an indirect consequence of the elevated Fe^{3+}/Fe^{2+} ratio of calc-alkaline magmas such as Rindjani, which promotes Fe^{3+} incorporation into magnetite at the expense of Fe^{2+}-Ti^{4+} pairs, such that increased oxygen fugacity will subdue Ti isotopic fractionation in global magmatic series. Similarly, we find negligible Fe isotopic fractionation in Rindjani bulk rocks and mineral separates, unlike previous studies. This is also likely due to the oxidized nature of the Rindjani differentiation suite, which leads to similar Fe^{3+}/Fe^{2+} ratios in melt and minerals and decreases overall mineral-melt Fe fractionation factors. Paired Ti and Fe isotopic analyses may therefore represent a powerful tool to assess oxygen fugacity during differentiation, independent from Fe^{3+} determinations of erupted samples.

1. Introduction

Titanium stable isotopes are fractionated to varying extents during igneous differentiation. These isotopic variations have consequently been used for tracing large scale differentiation processes such as the formation of Earth's continental crust (Greber et al., 2017b; Deng et al., 2018; 2019; Aarons et al., 2020; Aarons et al., 2021b) and lunar magma ocean crystallization (Millet et al., 2016; Greber et al., 2017a; Rzehak et al., 2021; 2022). In addition to being an abundant element, Ti is refractory, relatively insoluble, and exists in a single oxidation state (4+) on Earth. These characteristics free Ti isotopes of many of the complications faced by stable isotopic systems of other elements that are moderately volatile, soluble, and/or redox-sensitive.

To date, Ti isotopes have helped shed light on wide-ranging topics such as the composition of the Archean crust and the onset of plate tectonics (Greber et al., 2017b; Deng et al., 2018; 2019; Aarons et al., 2020), the differentiation histories of the Moon and Mars (Millet et al., 2016; Greber et al., 2017a; Deng et al., 2020; Rzehak et al., 2021; 2022), the history of continental topography and biological evolution (Saji et al., 2023), and sediment provenance studies (Greber et al., 2017b; Klaver et al., 2021; Heard et al., 2021; He et al., 2022). All these studies build on the observation that Ti isotopes are fractionated during magmatic differentiation, prompting continued interest in understanding the drivers of Ti isotopic fractionation in igneous systems.

Titanium stable isotopes are fractionated during magmatic differentiation primarily because Ti resides in higher coordination in Fe-Ti oxides (6-fold) than in silicate melt (mixtures of 4-, 5-, and 6-fold; (Farges et al., 1996; Farges and Brown, 1997), resulting in light isotopic enrichments in Fe-Ti oxides relative to melts at equilibrium (Millet et al., 2016; Leitzke et al., 2018; Johnson et al., 2019; Wang et al., 2020;

* Corresponding author at: Department of Geosciences, University of Arizona, Tucson, AZ, USA.
E-mail address: aleishajohnson@arizona.edu (A.C. Johnson).

https://doi.org/10.1016/j.gca.2023.06.016
Received 14 December 2022; Accepted 15 June 2023
Available online 22 June 2023

Aarons et al., 2021a; Hoare et al., 2022). Mineral separates from igneous rocks, such as Fe-Ti oxides, are indeed isotopically light compared to coexisting silicate melts and minerals, and the crystal fractionation of these oxides drives the Ti isotopic evolution of the melt (Johnson et al., 2019; Greber et al., 2021; Nie et al., 2021; Hoare et al., 2022).

A unique feature of Ti isotopes is that they appear to fractionate to different extents in magmas originating from different tectonic settings. Relatively dry, reduced, Ti-rich magmas tend to produce the most isotopically fractionated differentiates, whereas Ti isotopes in hydrous, oxidized, Ti-poor magmas tend to be less fractionated, even when the magmas are highly differentiated (Greber et al., 2017b; Deng et al., 2019; Johnson et al., 2019; Hoare et al., 2020; Zhao et al., 2020; Hoare et al., 2022).

There are several proposed mechanisms to explain why calc-alkaline magmas experience less Ti isotopic fractionation. Their increased water content suppresses plagioclase crystallization relative to other minerals, allowing melt SiO_2 to increase more quickly for a given degree of crystal fractionation. Calc-alkaline magmas also have higher oxygen fugacity, which tends to promote earlier crystallization of Fe-Ti oxides. These phenomena play a role, but cannot solely account for the more subdued Ti isotopic fractionation documented in calc-alkaline magma series compared to other magma series (Aarons et al., 2021a). Another important factor that can influence Ti isotopic fractionation is that Fe-Ti oxides have variable mineral-melt fractionation factors depending on their composition, which can modulate Ti isotopic fractionation during magmatic differentiation (Hoare et al., 2020; 2022). It was also hypothesized that increasing melt polymerization in high SiO_2 melts could exert a control over mineral-melt fractionation factors over the course of differentiation (Deng et al., 2019; Aarons et al., 2021a). To test these hypotheses and develop a quantitative understanding of Ti isotopic fractionation during magmatic differentiation, it is important to establish the fractionation factors between Fe-Ti oxides and silicate melt, where very little data for natural samples exist.

Like Ti stable isotopes, Fe stable isotopes also fractionate during magmatic differentiation (Teng et al., 2008; Schuessler et al., 2009; Sossi et al., 2012; Weyer and Seitz, 2012; Du et al., 2022). Iron is an abundant element in terrestrial magmas and is a major component of both the silicate and oxide minerals. Unlike Ti however, Fe is redox-sensitive, existing as both Fe^{2+} and Fe^{3+} in melts and minerals. This characteristic is responsible for most of the isotopic fractionation Fe experiences, because the bonding environment of Fe^{3+} in melts and minerals is stronger than Fe^{2+}, leading Fe^{3+}-rich minerals to concentrate heavier Fe isotopes (Dauphas et al., 2012; Roskosz et al., 2006). The evolution of Fe isotopes within melts can therefore record the relative removal rates of Fe^{2+} *vs.* Fe^{3+} in crystallizing minerals, providing a window into the redox conditions experienced during differentiation.

To explore the utility of paired Ti and Fe stable isotopes for understanding compositional and redox controls during magmatic differentiation, specifically in more oxidized calc-alkaline magmas where fewer data exist, we collected isotopic data from bulk samples and mineral separates of the calc-alkaline differentiation suite from the Rindjani Volcano, Indonesia. These data allow us to quantify mineral-melt fractionation factors over the course of magmatic differentiation and possible magma mixing, in a system with relatively well constrained temperature, melt composition, and mineralogy.

2. Materials and methods

2.1. Samples

Samples used in this study are lavas from Mount Rindjani, located on the island of Lombok in Indonesia. Mount Rindjani is situated in the central Sunda Arc, where the Indo-Australian plate subducts beneath the Eurasian plate. The lavas range in age from Pleistocene to present, with compositions spanning high-Al basalt, andesite, high-K andesite and trachy-andesite, and trachyte (Fig. 1). Lavas from Mount Rindjani originated in the sub-arc mantle and fall along the calc-alkaline differentiation trend. Although calc-alkaline magmas often show evidence for assimilation and mixing, which can complicate interpretations (e.g., Grove and Brown, 2018), available evidence, such as Sr isotopic data, suggests that these lavas experienced limited crustal contamination during ascent and emplacement (Whitford et al., 1978; Foden, 1983), and therefore provide a suitable case study to examine the effects of fractional crystallization on Ti and Fe isotopes in a calc-alkaline differentiation series.

For this study, 24 bulk whole rock powders were analyzed for their Fe and Ti stable isotopic compositions. Fresh rock samples were broken into 3–4 cm chips using a rock hammer, and the chips were crushed using a steel jaw crusher at the University of California – Santa Barbara. These chips were then pulverized in an alumina shatterbox on a SpexTM mill. The shatterbox was cleaned between samples using pure quartz sand followed by rinsing and drying with ethyl alcohol.

Mineral separates were also prepared from six crushed bulk samples for Fe and Ti stable isotopic analyses. First, 10 to 20 g of bulk sample was crushed and sieved in water to obtain a 50 to 185 μm size fraction. This size fraction underwent density separation in methylene iodide (MeI, density 3.32 g/cm^3) to separate two fractions enriched in (*i*) high density Fe-Ti oxides and (*ii*) silicate minerals and glass. Weights of each mineral

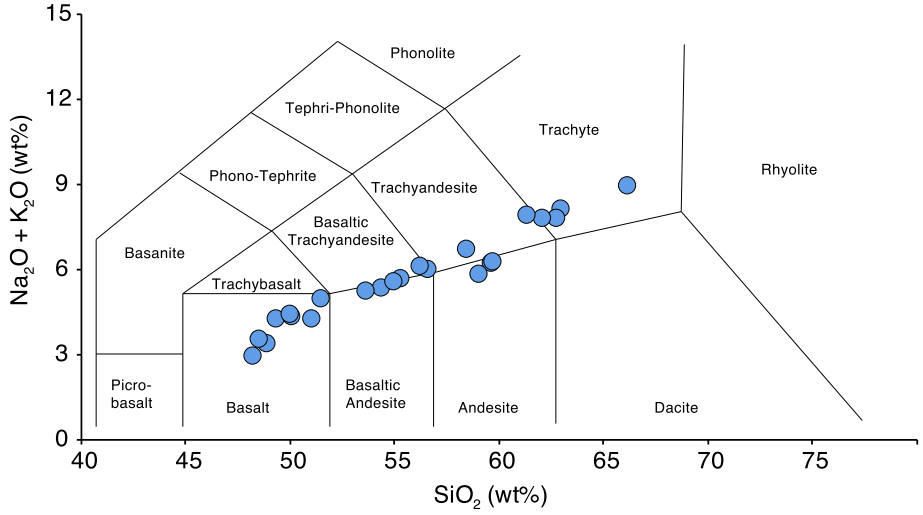

Fig. 1. Total alkali silica diagram (after Le Maitre et al., 2005) of the Rindjani differentiation suite studied here (data from Foden, 1983).

separate were recorded. Aliquots of each mineral separate were mounted in epoxy for petrographic and geochemical characterizations.

2.2. Petrographic characterization

Petrographic description of each of the samples is provided in the appendix. Modal percentages of phenocrysts were determined optically by visual estimation of thin sections at UCSB. Samples are dominantly glassy/fine-grained with phenocrysts making up 10 to 45% of each sample (unless otherwise noted, all modal fractions are in volume, Fig. 2). Early crystallizing phases include olivine, clinopyroxene, and plagioclase. Following the appearance of magnetite in more differentiated samples, orthopyroxene is observed while olivine is no longer present. In andesitic samples, amphibole is observed along with plagioclase, clinopyroxene, and magnetite. Fe-Ti oxides, when present in the differentiation suite, range between 1 and 5% of the sample and are typically unzoned grains of magnetite; the exception to this observation are two samples (LO-13 and LB-53) where magnetite grains contain exsolution lamellae of ilmenite.

Scanning electron microscopy (SEM) backscattered electron (BSE) images and energy-dispersive spectroscopy (EDS) spectra of individual minerals were collected for each mineral separate. Samples mounted in epoxy were analyzed with the TESCAN LYRA3 field-emission SEM at the University of Chicago. The SEM-EDS was operated at a 15 kV accelerating voltage and beam intensity of 0.26 nA. Following calibration with a cobalt standard, elemental maps and point spectra were collected with EDS to measure the composition and volume fractions of the minerals in the density separates.

2.3. Major and trace elements

All samples (n = 36 corresponding to the 24 bulk powders and 6+6 low- and high-density mineral separates) were analyzed for major and minor elements using a Thermo ICAP-Q quadrupole ICP-MS at Arizona State University. Aliquots of the samples were digested on a hot plate in a 10:1 HNO_3:HF mixture, followed by concentrated HCl to dissolve fluorides. Samples that were not fully digested by this procedure were further processed in a parr bomb containing a 2:1 HNO_3:HF mixture until dissolution was complete. Analyses were conducted using a multielement (Sc, Ge, Y, In, Bi) internal standard and in-house multielement external calibration standards. Based on repeat analysis (n = 4) of the in-run multielement standard, typical measurement precision was better than 5%. Concentrations of geostandards BIR-1, RGM-1, and G-2 were analyzed by the same method and were typically within ~10% of certified concentrations (see supplement). All ICP-MS data are presented in the supplement, along with major and minor element analyses of the same samples from Foden (1983) and XRF and LA-ICP-MS data generated at the University of California – Santa Barbara that was reported in Toc (2018), where the XRF data were acquired on fused glass beads at Pomonoa College and LA-ICP-MS data for trace elements collected on the same glass beads at the UC Santa Barbara LASS facility. Unless otherwise specified, data in the main text, tables, and figures are XRF data for major elements, and the ICP-MS data for trace elements.

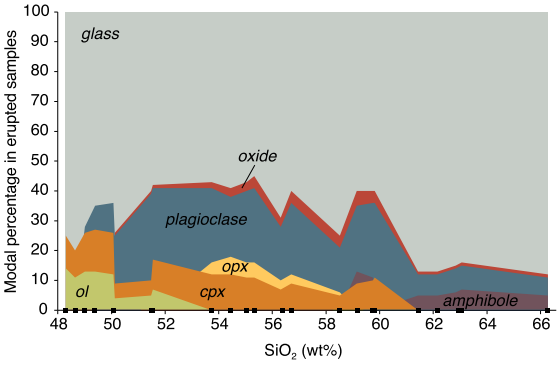

Fig. 2. Modal percentage of phenocrysts (ol = olivine, cpx = clinopyroxene, opx = orthopyroxene, oxide = magnetite, plagioclase, amphibole) in glassy/fine-grained groundmass. Black squares along the x axis are individual samples (SiO_2 from (Foden, 1983).

2.4. Iron and titanium isotopic analyses

Twenty-four bulk samples and twelve mineral separates were prepared for Ti and Fe isotopic analysis at the Origins Lab of the University of Chicago. For Ti isotopic analyses, ~0.1 g of each sample (≥10 μg Ti) was weighed out with ~0.6 g of $LiBO_2$ and three drops of LiBr non-wetting solution into a graphite crucible and melted for 10 min at 1150 °C in air for flux fusion (Greber et al., 2017a). A shard from the flux fusion bead was weighed into a PFA beaker with ^{47}Ti-^{48}Ti double-spike in a 48:52 spike-sample ratio (Millet and Dauphas, 2014). The sample with double spike added was dissolved in 10 mL of 3 M HNO_3 at 130 °C and sonicated until fully dissolved. This dissolution procedure ensures Ti isotopic equilibration between the sample and double-spike. As a precautionary step to avoid secondary precipitates from clogging the columns, the samples were centrifuged in 2 mL centrifuge tubes immediately prior to column chemistry, with the upper 1.9 mL going into the column and 0.1 mL stored. Column chemistry followed the method of Millet and Dauphas (2014), which first uses a 10 mL Bio-Rad column and a prepacked 2 mL Eichrom TODGA resin cartridge (50–100 μm) to remove most matrix elements. This step was followed by two rounds of a 5 mL microcolumn (3.2 mm ID × 10 cm) filled with 0.8 mL of AG1-X8 200–400 mesh resin to remove remaining Mo and high field strength elements (Nb, Ta, W) (Zhang et al., 2011). Final solutions were dried down and brought up in 2% HNO_3 with HF to match concentrations and perform Ti isotopic analyses.

For Fe isotopic analyses, ~10 mg of each sample (≥250 μg Fe) was weighed into PFA beakers and digested in a 2:1 mixture of HF:HNO_3 with two drops of $HClO_4$ at 130 °C, followed by dry down and digestion in a 3:1 mixture of HCl:HNO_3 with 3–5 drops of $HClO_4$, and finally digestion in a 2:1 mixture of HCl:HNO_3 with two drops of $HClO_4$. Once dissolved, the samples were dried down and re-dissolved in 6 M HCl for column chemistry. For Fe purification, we followed the method of Dauphas et al. (2009), where samples were twice put through a Bio-Rad column with 1.0 mL of AG1-X8 200–400 mesh resin for purification. Purified Fe samples were brought up in a final stock solution of 2% HNO_3 for analysis.

Measurements were performed on a Neptune MC-ICPMS at the Origins Lab of the University of Chicago. Titanium isotopic analyses were done using an Apex Q desolvating nebulizer attached to a Spiro heated membrane desolvation module and measured in medium resolution. Isotopes ^{46}Ti, ^{47}Ti, ^{48}Ti, ^{49}Ti, and ^{50}Ti were measured simultaneously in muli-collection. Isotopes ^{46}Ti and ^{50}Ti were measured as flat top shoulders to resolve interferences from $^{30}Si^{16}O^+$ on $^{46}Ti^+$ and $^{36}Ar^{14}N^+$ on $^{50}Ti^+$. All samples were measured using sample standard bracketing with standards doped with double-spike in the same 48:52 ratio as the samples. Concentrations were matched within 10% at ~200 ppb and run at a signal on $^{48}Ti^+$ of 10 to 15 V on a 10^{11} Ω amplifier. Samples were measured using 40 integrations of 4.194 s each. We report the Ti isotopic composition of each sample in δ^{49}Ti notation, which is the permil deviation from the ^{49}Ti/^{47}Ti ratio of the Origins Laboratory Ti reference material (OL-Ti), a composition that is close to chondrites (Greber et al., 2017a),

$$\delta^{49}\mathrm{Ti}(\%) = \left[\frac{(^{49}\mathrm{Ti}/^{47}\mathrm{Ti})_{\mathrm{sample}}}{(^{49}\mathrm{Ti}/^{47}\mathrm{Ti})_{\mathrm{OL-Ti}}} - 1\right] 1000. \quad (1)$$

The concentration-matched bracketing standards were spiked with the same double-spike as the samples and went through the same data reduction procedure. Measured data were corrected for potential Ti

isotopic mass fractionation during the purification and isotopic measurements using the double-spike technique described in Millet and Dauphas (2014). Uncertainty is reported at the 95% confidence interval (CI), which is calculated from the reproducibility of 9 or more replicate measurements. Long term reproducibility was assessed from the standard deviation of all in-run OL-Ti bracketing standards and was found to be ±0.02‰. Geostandards were also analyzed and generally match literature values (Aarons et al., 2020) within error: δ^{49}Ti = +0.436 ± 0.009‰ for G-3 (*vs.* +0.431 ± 0.043‰), −0.032 ± 0.008‰ for BIR-1 (*vs.* −0.047 ± 0.005‰), and +0.026 ± 0.009‰ for BHVO-2 (*vs.* + 0.028 ± 0.005‰).

Iron isotopic analyses used a dual cyclonic-Scott spray chamber introduction system and were measured in medium resolution on flat top peak shoulders to avoid ArN^+, ArO^+, and $ArOH^+$ interferences. All samples were measured using sample standard bracketing with IRMM-524, which has the same Fe isotopic composition as IRMM-014 (Craddock and Dauphas, 2011). Concentrations were matched within 5% at ~1 ppm and run at a $^{56}Fe^+$ intensity of 5 to 6 V on a 10^{11} Ω amplifier. Samples were measured using 25 integrations of 4.194 s each. The Fe isotopic composition of each sample is reported in δ^{56}Fe notation, which is the permil deviation from the $^{56}Fe/^{54}Fe$ ratio of IRMM-524/IRMM-014,

$$\delta^{56}\mathrm{Fe}(\%) = \left[\frac{(^{49}\mathrm{Fe}/^{47}\mathrm{Fe})_{\mathrm{sample}}}{(^{49}\mathrm{Fe}/^{47}\mathrm{Fe})_{\mathrm{IRMM-014}}} - 1\right]1000. \quad (2)$$

Uncertainty is reported at the 95% confidence interval, which incorporates uncertainty from the long-term reproducibility of bracketing standards (±0.032 to ± 0.058‰) as well as error from unaccounted analytical fractionation (±0.012‰) (Dauphas et al., 2009). Geostandards were also analyzed and match with literature values within error: +0.080 ± 0.058‰ for AGV-2 (*vs.* a literature value of +0.105 ± 0.011‰; +0.130 ± 0.038‰), +0.093 ± 0.035‰ for BHVO-2 (*vs.* +0.114 ± 0.011‰), +0.107 ± 0.034‰ for BCR-2 (*vs.* +0.091 ± 0.011‰; +0.079 ± 0.043‰), and IF-G + 0.590 ± 0.058‰ for IF-G (*vs.* +0.639 ± 0.013‰; +0.640 ± 0.058‰) (Craddock and Dauphas, 2011; Dideriksen et al., 2006; Weyer et al., 2005; Rouxel et al., 2005).

3. Results

The high-density mineral separates are primarily composed of Fe-Ti oxides (low-Ti magnetite), and silicate glass, with varied amounts of mafic silicate minerals (olivine, pyroxene, or amphibole, depending on the stage of differentiation) (Fig. 3). The Fe concentration is higher in all mafic minerals (10–80 wt% FeO) compared to the glass (3–7 wt% FeO), with the greatest enrichment seen in magnetite. Titanium is enriched in magnetite (~10 wt% TiO_2) with lower concentrations observed in pyroxene and silicate glass (<1 wt% TiO_2). Low density mineral separates are primarily composed of silicate glass and plagioclase, with trace mafic minerals and oxides (Fig. 4).

Select major elements and Ti and Fe isotopic analyses for all samples are presented in Tables 1–2 and Figs. 5–8 (see Supplement for full dataset). To track Fe and Ti isotopic evolution as a function of differentiation, we compare bulk rock isotopic values to both SiO_2 and removal of Ti compared to an incompatible element, thorium. For example, if we assume that the TiO_2/Th ratio of the least differentiated sample, LB-43, represents the TiO_2/Th ratio of the parental melt, the TiO_2/Th ratio of differentiated samples decreases as crystal fractionation preferentially removes TiO_2 compared to highly incompatible Th. We use TiO_2/Th ratios to estimate the extent of Ti removal by writing

$$f_{\mathrm{Ti}} = \left[\frac{(\mathrm{TiO_2/Th})\mathrm{sample}}{(\mathrm{TiO_2/Th})\mathrm{LB-43}}\right], \quad (3)$$

where f_{Ti} represents the remaining Ti in the system. The fraction of Fe remaining in the melt was calculated in a similar manner,

$$f_{\mathrm{Fe}} = \left[\frac{(\mathrm{Fe_2O_3/Th})\mathrm{sample}}{(\mathrm{Fe_2O_3/Th})\mathrm{LB-43}}\right], \quad (4)$$

Note that calculation of f_{Ti} and f_{Fe} by normalization to Th assumes that it behaves as a purely incompatible element, and was not replenished by assimilation or magma injection, and was not significantly removed by trace Th-rich phases such as apatite. Those assumptions are reasonable because normalization to other incompatible elements, such as U, yield similar fractions of Fe and Ti remaining (Figs. 5 and 6).

In Fig. 5A-B we show that Fe_2O_3* and fraction of remaining Fe (normalized to Th and U) continuously decrease relative to SiO_2 content. Early crystallizing phases include olivine and clinopyroxene, followed by increasing proportions of plagioclase, with magnetite observed in samples with >50 wt% SiO_2. Olivine is no longer observed above 52 wt % SiO_2 and orthopyroxene is observed instead. In samples > 59 wt% SiO_2, trace amphibole is found instead of orthopyroxene, while plagioclase, clinopyroxene, and magnetite are still present. As shown in Fig. 5B, the continual removal of Fe_2O_3 results in <10% of the initial melt Fe remaining in samples with >62 wt% SiO_2.

Despite continual removal of Fe by fractional crystallization, we

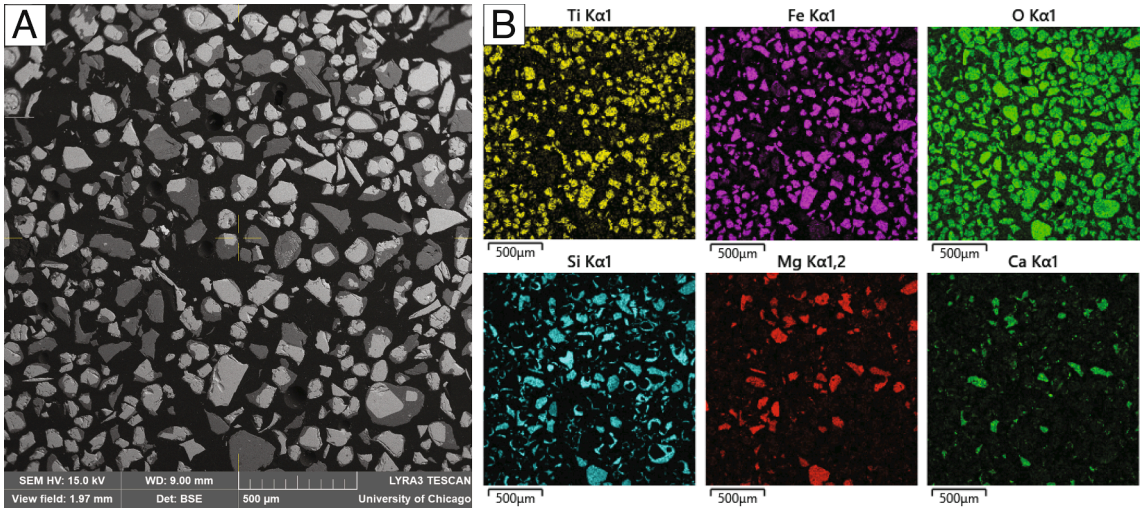

Fig. 3. (A) Example back-scattered electron (BSE) image of a high density mineral separate (LBK-8) composed primarily of magnetite (light gray) and quenched silicate glass (medium gray). (B) EDS map spectra indicate trace pyroxene (Ca), and in other cases olivine (Mg) and trace amphibole (Ca, Mg), were also present in the high density mineral separates, but had comparatively much lower Ti and Fe contents than magnetite (Ti, Fe spectra).

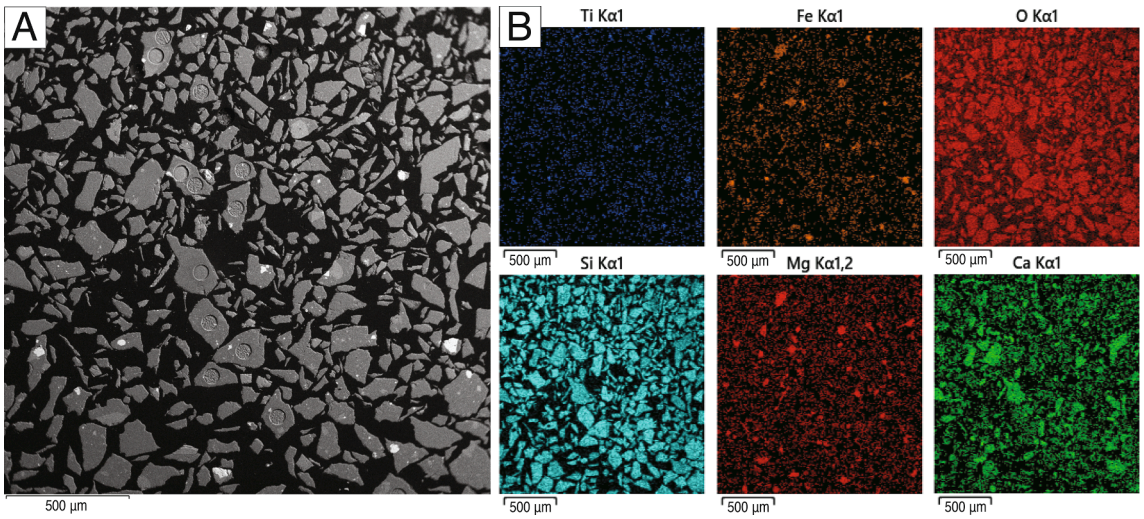

Fig. 4. (A) Example BSE image of a low density mineral separate (LBK-8) composed primarily of quenched silicate glass and plagioclase (medium gray) with trace magnetite (light gray). (B) EDS map spectra indicate trace magnetite (Ti, Fe spectra), trace pyroxene (Mg, Fe spectra), and in other cases trace amphibole (Ca, Mg), were also present in the low density mineral separates.

Table 1
Major element, Ti, and Fe stable isotopic data for bulk samples.

Sample	SiO_2 (wt%)	TiO_2 (wt%)	Fe_2O_3* (wt%)	f_{Ti}	f_{Fe}	δ^{49}Ti (‰)	95%CI (‰)	δ^{56}Fe (‰)	95%CI (‰)
LB-43	48.14	0.77	10.42	1.00	1.00	0.005	0.011	0.035	0.032
LB-34	48.85	0.87	11.20	0.77	0.84	0.006	0.021	0.068	0.053
LO-46	49.00	0.96	11.22	0.75	0.67	−0.025	0.013	0.106	0.053
LB-33	49.69	0.93	10.22	0.64	0.52	−0.007	0.018	0.053	0.032
LO-45	50.30	0.94	10.24	0.56	0.45	0.081	0.016	0.043	0.035
LO-14	50.65	1.10	10.69	1.07	0.77	0.017	0.012	0.066	0.053
LO-11	52.17	1.17	10.12	0.40	0.26	0.061	0.017	0.055	0.035
LO-10	51.10	1.16	10.18	0.38	0.25	0.033	0.017	0.048	0.034
LBK-2	54.48	0.93	8.83	0.42	0.30	0.017	0.021	0.143	0.032
AR-6	55.49	0.95	8.64	0.39	0.26	0.088	0.013	0.051	0.032
LBK-4	56.25	0.93	8.08	0.37	0.24	0.128	0.020	0.095	0.034
LBK-6	55.75	0.91	8.08	0.36	0.24	0.087	0.018	0.044	0.034
LB-53	57.52	0.85	7.34	0.24	0.16	0.126	0.015	0.058	0.032
LO-47	56.55	0.90	7.57	0.35	0.22	0.114	0.012	0.012	0.035
LB-49	59.60	0.79	6.45	0.19	0.12	0.187	0.012	0.061	0.035
LO-13	60.88	0.71	6.40	0.33	0.22	0.167	0.012	0.081	0.035
LBK-8	62.33	0.73	6.29	0.17	0.11	0.168	0.019	0.031	0.034
LBK-7	60.09	0.78	6.90	0.19	0.13	0.124	0.013	0.031	0.034
LO-52	64.55	0.62	4.07	0.12	0.06	0.292	0.017	0.061	0.032
LO-5	64.64	0.64	4.09	0.13	0.06	0.302	0.015	0.095	0.053
LBK-9	64.40	0.63	4.33	0.12	0.06	0.303	0.014	0.100	0.053
LBK-10	64.62	0.61	4.06	0.15	0.08	0.319	0.019	0.069	0.053
LO-38	67.80	0.57	3.02	0.09	0.04	0.457	0.021	0.101	0.053
LO-37	67.69	0.58	3.19	0.08	0.03	0.472	0.017	0.065	0.053

Footnote: Major elements reported here are XRF data measured at UCSB (see supplement for comparison with data from Foden, 1983). Total iron reported as Fe_2O_3*. All isotopic data are the average of at least nine standard-sample-standard bracket measurements, with the uncertainties reported as 95% confidence intervals.

observe no trend in δ^{56}Fe values as a function of differentiation (Fig. 5C). This observation is consistent with the δ^{56}Fe values of the mineral separates, which show no significant isotopic offset from the whole rock (Fig. 5D). While instantaneous mineral-melt isotopic fractionation can be amplified by Rayleigh distillation effects, no fractionation is observed in highly differentiated samples where <10% of initial melt Fe remains.

Fig. 6B shows that TiO_2 is continuously removed relative to Th. This observation is less apparent when comparing TiO_2 to SiO_2, where TiO_2 abundance initially increases during the crystallization of olivine and clinopyroxene (Fig. 6A). This is because, early-on, TiO_2 is incompatible and is removed at a slower pace than another major element such as SiO_2 that controls the fraction of melt remaining (Fig. 6A). Following the crystallization of magnetite, TiO_2 abundance continuously decreases. However, it is important to note that by the first appearance of magnetite, ~60% of the initial melt Ti was already removed, likely as a trace constituent of clinopyroxene (Fig. 6B).

During initial Ti removal when olivine and pyroxene are crystallizing, very little Ti isotopic fractionation is seen (Fig. 7A-B). Following the appearance of magnetite in samples with >52 wt% SiO_2, δ^{49}Ti values steadily increase, both as a function of SiO_2, and progressive Ti removal (Fig. 7A-B). At 67–68 wt% SiO_2, samples reach a maximum δ^{49}Ti value of 0.47‰, similar to other calc-alkaline differentiation suites (Greber et al., 2017b; Hoare et al., 2020; 2022). In Fig. 7B, the slope between δ^{49}Ti and the negative natural logarithm of the fraction of Ti remaining in the melt indicates the "net" fractionation factor imparted by the bulk crystallizing assemblage. The calculated slope inferred from linear regression of δ^{49}Ti against $-\ln f_{Ti}$ is around 0 prior to oxide crystallization, and +0.19 after oxide crystallization. The "net" fractionation factor

Table 2
Ti and Fe stable isotopic data and TiO_2 concentrations of high density (HD) and low density (LD) mineral separates.

Sample	f_mass	TiO_2 (wt%)	$\delta^{49}Ti$ (‰)	95 CI (‰)	$\delta^{56}Fe$ (‰)	95 CI (‰)	Corrected $\delta^{49}Ti$ (‰)	95 CI (‰)	$\Delta^{49}Ti$ (‰)	95 CI
LO-11 LD	0.927	1.17	0.051	0.015	0.028	0.058	0.10	0.06		
LO-11 HD	0.073	1.62	−0.268	0.015	0.026	0.058	−0.28	0.03		
oxides		9.85							0.38	0.07
Temp = 980 °C										
AR-6 LD	0.925	0.63	0.171	0.011	−0.008	0.058	0.29	0.08		
AR-6 HD	0.075	4.38	−0.185	0.011	0.003	0.058	−0.19	0.02		
oxides		9.68							0.48	0.09
Temp = 920 °C										
LB-53 LD	0.974	0.75	0.179	0.008	0.028	0.058	0.21	0.04		
LB-53 HD	0.026	4.62	−0.031	0.018	0.050	0.058	−0.04	0.04		
oxides		9.76							0.25	0.05
Temp = 950 °C										
LO-13 LD	0.974	0.56	0.220	0.022	−0.001	0.058	0.35	0.08		
LO-13 HD	0.026	5.85	−0.030	0.013	0.092	0.058	−0.04	0.03		
oxides		7.75							0.44	0.08
Temp = 910 °C										
LBK-8 LD	0.960	0.58	0.195	0.021	0.021	0.058	0.24	0.06		
LBK-8 HD	0.040	5.03	−0.045	0.015	0.018	0.058	−0.050	0.03		
oxides		10.69							0.35	0.07
Temp = 900 °C										
LO-38 LD	0.992	0.50	0.482	0.019	0.000	0.058	0.73	0.15		
LO-38 HD	0.008	10.06	−0.052	0.009	–	–	−0.05	0.02		
oxides		14.86							0.58	0.15
Temp = 895 °C										

Footnote: Major elements reported here and in the supplement for mineral separates are ICPMS data measured at ASU. All isotopic data are the average of at least nine standard-sample-standard bracket measurements, with the uncertainties reported as 95% confidence intervals.

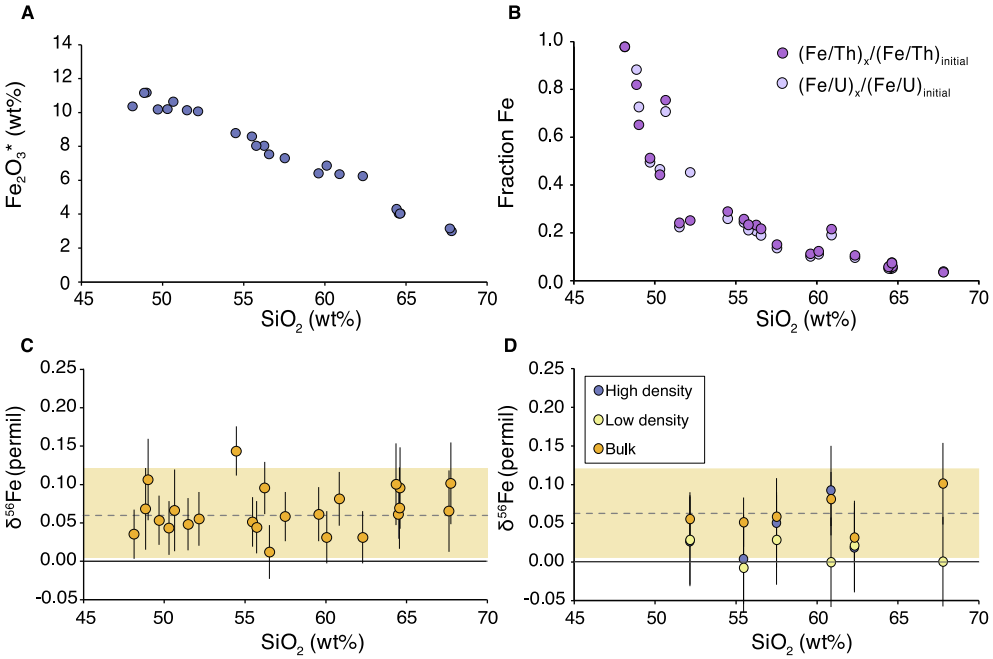

Fig. 5. (A) Bulk rock Fe_2O_3* (total iron) plotted against SiO_2. (B) Fraction of initial Fe remaining in the melt plotted against SiO_2. Fraction Fe remaining was calculated by assuming Th and U behaved as perfectly incompatible elements and calculating $(Fe_2O_3/U,Th)/(Fe_2O_3/U,Th)_{initial}$ for each sample. (C) Bulk rock $\delta^{56}Fe$ values plotted against SiO_2; uncertainties are 95% CI. The weighted average of all bulk rock data is plotted as a dashed line with a 95% CI error envelope. (D) $\delta^{56}Fe$ values of bulk rock (orange) and mineral separates (blue and yellow) plotted against SiO_2; uncertainties are 95% CI.

of approximately +0.2‰ after the onset of oxide crystallization is similar to values obtained for other calc-alkaline suites (Millet et al., 2016; Hoare et al., 2020).

In Fig. 8A, $\delta^{49}Ti$ values of the high- and low-density mineral separates are plotted with their corresponding bulk rock value against whole rock SiO_2. The low-density mineral separates are isotopically heavy compared to the high-density separates, with an isotopic offset ranging from +0.21‰ to +0.53‰. Low-density mineral separates are very similar to bulk rock values, which is to be expected as these are poorly crystalline samples with the most of the Ti hosted in silicate glass (quenched melt). Both the low- and high-density mineral separates are partial mixtures of the main carriers of Ti. Titanium is present primarily in Fe,Ti-oxide, clinopyroxene, and glass (melt). We use the approach of Johnson et al. (2019) to build mixing lines that extrapolate the $\delta^{49}Ti$ values of pure oxides and silicate using the K_2O/TiO_2 and CaO/TiO_2 ratios of the pure phases, mineral separates, and bulk rock samples. Because clinopyroxene is present in both low- and high- density mineral separates, and is a minor but non-negligible carrier of Ti that is treated here as part of the melt, these mineral pairs might be best thought of as silicate-oxide pairs; however, due to the similarity between clinopyroxene and silicate melt with respect to TiO_2 content and Ti isotopic composition, we expect that they are nearly identical to melt-oxide pairs. Using a weighted regression and propagating the errors to the extrapolated pure phases, the resulting corrected values have greater

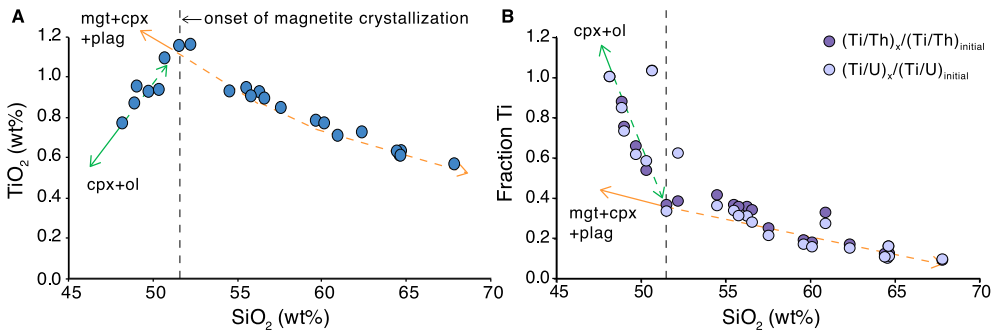

Fig. 6. (A) Bulk rock TiO_2 plotted against SiO_2. Magnetite first appears at peak TiO_2 contents near ~52 wt% SiO_2. (B) Fraction of initial Ti remaining in the melt plotted against SiO_2. The fraction of Ti remaining in the melt (f_{Ti} in Eq. (4) was calculated by assuming Th and U behaved as perfectly incompatible elements and calculating $(TiO_2/Th)/(TiO_2/Th)_{initial}$ for each sample. At the first appearance of magnetite, ~40% of the initial Ti remained compared to the least differentiated sample (LB-43).

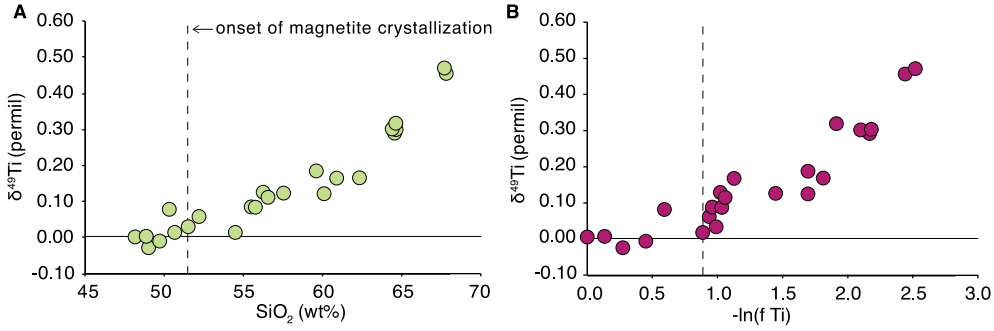

Fig. 7. (A) Bulk rock $\delta^{49}Ti$ values plotted against SiO_2; uncertainties are 95% CI and are smaller than the symbol size. The first non-zero $\delta^{49}Ti$ value appears above 50 wt% SiO_2, near the appearance of magnetite in the samples. (B) Bulk rock $\delta^{49}Ti$ values plotted against progressive Ti removal, quantified as $-\ln((TiO_2/Th)/(TiO_2/Th)_{initial})$, where the slope indicates the "net" fractionation factor imparted by mineral crystallization.

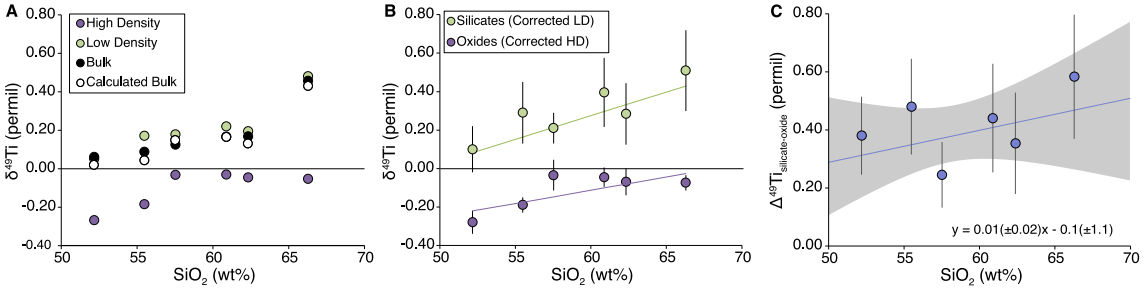

Fig. 8. (A) Measured $\delta^{49}Ti$ values of bulk rock (black) and mineral separates (purple and green) plotted against SiO_2; uncertainties are 95% CI. (B) Corrected $\delta^{49}Ti$ values of high- and low-density (HD and LD) mineral separates plotted against SiO_2, which represent $\delta^{49}Ti$ of silicates and Fe-Ti oxides, respectively (see text for details of correction). Uncertainties are 95% CI, with more significant corrections resulting in larger propagated errors. (C) $\Delta^{49}Ti_{silicate\text{-}oxide}$ values (the difference between $\delta^{49}Ti_{silicate}$ and $\delta^{49}Ti_{magnetite}$) plotted against SiO_2.

isotopic offsets, ranging from +0.25 to +0.58‰ (Fig. 8B), which represent discrete silicate-oxide fractionation factors.

To calculate the relevant quench temperature of each silicate-oxide pair, we used rhyolite MELTs modeling and the bulk composition of each sample (Gualda et al., 2012; Ghiorso and Gualda, 2015) to identify the temperature at which each bulk assemblage reached the measured crystal:glass ratio (Fig. 2; Table 2). We assume 3 wt% H_2O, unbuffered oxygen fugacity that began at QFM, and starting temperature and pressure of 1200 °C and 1 kb (consistent with estimates by Foden, 1983, as well as P and H_2O estimates by Métrich et al. (2017) based on melt inclusion analyses by Vidal et al., 2016). Cooling/crystallization was performed in isenthalpic decrements of −50 J at constant pressure. As a quality check, model runs were only accepted if they reproduced the crystal assemblage observed in the samples; the most stringent of these controls was whether the model correctly predicted the appearance of magnetite, which appears after olivine, plagioclase, and pyroxene. Modification of the above parameters (ex: QFM to QFM + 1; 2 to 3 wt% H_2O; 1 to 5 kb) resulted in temperature estimates varying ±10 °C, but this is likely not the largest source of uncertainty. If, for example, the lavas left behind crystal cargo and quenched before re-equilibration, the samples would overestimate the glass/crystal ratio and overestimate quench temperature. The MELTs models indicate that decreasing the glass/crystal ratio by 10% decreases the estimated eruption temperature by 30 to 40 °C. The exsolution lamellae observed within magnetite in two samples (LO-13 and LB-53) indicate that at least some lavas were not instantaneously quenched, as we would like to assume, and thus our approach may overestimate quench temperature. Previous calculations estimating the closure temperature of Ti in oxides for volcanic samples indicated closure temperatures well above the eruption temperatures estimated here (Johnson et al., 2019), which is supported by the absence of zoning or Ti diffusion profiles in the oxides near their melt boundaries. It therefore seems reasonable to assume that the estimated eruption temperatures represent Ti closure temperatures, but with an expanded uncertainty of ±20 °C to account for possible modification of the glass/crystal ratio during lava transport and eruption. Encouragingly, our temperature estimates based on sample crystallinity (895 to

980 °C) are consistent with temperature estimates from previous Rindjani studies that used optical thermometry of melt inclusions (900 to 990 °C) (Métrich et al., 2017).

Using these modeled quench temperatures, we plot silicate-oxide fractionation factors against $10^6/T^2$ and include data from *ab initio* studies as well as other published melt-magnetite pairs (Fig. 9). All data plot within error of the weighted average 0.55 ($\pm$0.09 2σ) $\times$ $10^6/T^2$. Our silicate-oxide fractionation factors agree most closely with the modeled melt-titanomagnetite pairs of Aarons et al. (2021a), and are also very similar to the average melt-ilmenite fractionation observed by Hoare et al. (2022).

4. Discussion

Titanium and Fe stable isotopes undergo fractionation during magmatic differentiation, due in part to the crystallization and removal of Fe-Ti oxides (Teng et al., 2008; Deng et al., 2019; Hoare et al., 2022; Zhao et al., 2022). Intriguingly, Fe and Ti isotopes fractionate differently in different magmatic series when indexed to differentiation proxies like bulk SiO_2. Addressing this problem requires a deeper understanding of the fractionation factors between Fe-Ti oxides and silicate melt that govern the overall evolution of the system, where limited data are available. In the following sections, we discuss our results in the context of Fe and Ti isotope systematics of other magmatic systems, the various drivers of isotopic fractionation in these settings, and potential future applications of paired Fe and Ti isotopic analyses.

4.1. Drivers of Ti isotopic fractionation during magmatic differentiation

4.1.1. Ti removal in oxides vs. silicates

The Ti isotopic fractionation in the Rindjani differentiation suite is tracked by (*i*) measuring silicate-oxide fractionation factors, which range from +0.25 to +0.58‰ (Fig. 8B-C), and (*ii*) deriving a "net" mineral-melt fractionation factor of +0.2 from the derivative of bulk δ^{49}Ti evolution after the onset of magnetite crystallization (Fig. 7B). The discrepancy in fractionation factors derived by these two methods indicates that, in our samples, Ti was removed from the melt during crystallization of both oxides and silicates. While oxides strongly fractionate Ti isotopes during crystallization, and remove Ti in significant quantities, Ti removed by silicates, such as clinopyroxene, experiences much less, if any, measurable isotopic fractionation and serves to mute the net fractionation factor compared to oxide-melt fractionation factors.

Results from *ab initio* calculations (Leitzke et al., 2018; Wang et al., 2020; Aarons et al., 2021a) as well as experiments (Rzehak et al., 2022) suggest that silicates such as clinopyroxene might incorporate isotopically heavy Ti isotopes compared to silicate melt. However, we see no evidence for Ti isotopic fractionation by clinopyroxene in the Rindjani magmatic suite, similar to other magmatic suites (Hoare et al., 2022). Before the onset of oxide crystallization and when clinopyroxene is the only significant Ti-bearing phase, we observe no measurable isotopic fractionation despite significant (~60%) Ti removal (Fig. 7B). This suggests that the Ti isotopic composition of clinopyroxene in this system is very similar to the melt. One possibility is that Rindjani clinopyroxene hosts Ti in a mixture of 4- and 6-fold coordination, mimicking the dominantly ~5-fold coordination of Ti in the melt (Leitzke et al., 2018). Little is known about what controls the distribution of Ti in clinopyroxene (although melt chemistry plays a role, see (Nazzareni et al., 2004), so it is difficult to say how characteristic this behavior is of other calc-alkaline or terrestrial systems.

Other silicates to consider are olivine and plagioclase, which primarily host Ti in 4-fold coordination and are therefore predicted to be isotopically heavy compared to silicate melt (e.g., Greber et al., 2021); however, partition coefficients for Ti in olivine and plagioclase indicate that for Rindjani magmas with $\leq$1 wt% TiO_2, olivine contains < 0.02 wt % TiO_2 and plagioclase contains < 0.1 wt% TiO_2, which is consistent with Ti measuring below the LOD for our SEM EDS mineral spectra. Even though there are samples where plagioclase is 20$\times$ greater in abundance compared to oxides, oxides have 200$\times$ more TiO_2, so plagioclase would account for <10% of Ti removal relative to oxides at any point in time. Because of this, plagioclase may contribute to decrease the net fractionation factors compared to oxide-melt fractionation factors, but likely plays a secondary role to Ti removal by clinopyroxene.

The discrepancy between silicate (melt, clinopyroxene, and plagioclase) - oxide fractionation factors and the net fractionation seen in the bulk rock is not observed to the same degree in anhydrous, Ti-rich melts (Deng et al., 2019; Johnson et al., 2019; Hoare et al., 2022), likely because their crystallizing assemblage includes ilmenite (~50 wt% TiO_2) and Ti removal is dominated by oxide crystallization. In the Rindjani suite, magnetite only contains ~10 wt% TiO_2 and ilmenite is only found as a subsolidus exsolution phase. Additionally, mass balance calculations using mineral mode data (see Fig. 2) indicate that clinopyroxene may account for up to 30% of total Ti removal when magnetite is crystallizing, with up to 10% additionally removed by plagioclase. The 'net' isotopic fractionation factor of $10^3\ln\alpha_{melt\text{-}solid}$ = 0.22‰ can be explained with 38% of the fractionation contributed by melt-pyroxene

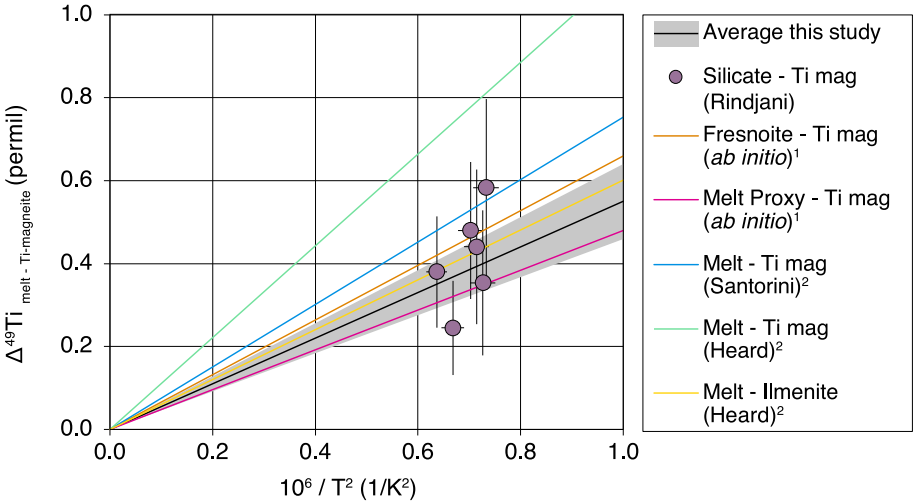

Fig. 9. Melt-magnetite fractionation factors for Rindjani mineral separates (purple circles, 95 CI; gray envelope is the weighted average) plotted as a function of temperature. For comparison, we include *ab initio* estimates of fresnoite ($Ba_2Ti(Si_2O_7)O$) and the melt proxy (a calculated mixture of 6-fold and 4-fold coordination) of Aarons et al. (2021a) (denoted ref. 1 in figure), as well as melt-magnetite and melt-ilmenite pairs from Hoare et al. (2022) (denoted ref. 2 in figure).

(±plagioclase) isotopic fractionation with $10^3\ln\alpha_{melt\text{-}cpx} = 0‰$, and 62% of the fractionation from melt-magnetite isotopic fractionation with $10^3\ln\alpha_{melt\text{-}magnetite} = 0.35‰$, averaged from Table 2. Thus, only 70% of Ti removed in crystallizing phases would have undergone significant isotopic fractionation by magnetite, reducing the net fractionation factor to the observed range of 0.2 to 0.3 permil. Aarons et al. (2021a), using Rhyolite-MELTS modeling, found much greater isotopic fractionation than seen in published δ^{49}Ti values for calc-alkaline differentiation series. Their MELTS modeling suggested that clinopyroxene stops crystallizing at around 57 wt% SiO_2 and accounts for less than 10% of total Ti removal. In the Rindjani lavas, we find that clinopyroxene crystallized until 62 wt% SiO_2 and accounts for nearly 30% of the total Ti that is removed, even when Fe-Ti oxides were crystallizing. This most likely explains the discrepancy between the observed Ti isotopic fractionation and MELTS modeling of Aarons et al. (2021a). This discrepancy is caused by the difficulty of modeling the crystallization of water-bearing melts, which can easily overestimate the abundance or Ti content of trace mineral phases such as Fe-Ti oxides.

4.1.2. Oxide mineralogy and oxygen fugacity

The greater role of silicates in determining the Ti budgets of arc magmas may be one reason why calc-alkaline suites experience less Ti isotopic fractionation than alkaline or tholeiitic suites (see also Hoare et al., 2022), but evidence was recently published that the composition of the oxides themselves also exerts a control on melt-oxide fractionation factors. Hoare et al. (2022) measured mineral-melt pairs for Ti-bearing magnetite, ilmenite, and rutile and found Ti-rich magnetite (~22 wt% TiO_2) produced the largest mineral-melt fractionation factors, followed by Ti-poor magnetite (~14 wt% TiO_2), followed by ilmenite and rutile. The minerals that drive heavy Ti isotopic enrichments in melts are the ones that are isotopically most fractionated and contain more titanium. Thus, Ti-rich melts that crystallize either Ti-rich magnetite (large fractionation and significant mass-balance leverage) and ilmenite (less isotopic fractionation but more mass-balance leverage) will rapidly remove Ti and strongly fractionate its isotopes, whereas Ti-poor calc-alkaline melts crystallizing Ti-poor magnetite will experience less isotopic fractionation.

The role of oxide composition in determining magnetite-melt fractionation factors becomes even more apparent when one compares the fractionation factors from Rindjani with magnetite-melt pairs from Santorini, Heard Island, and the Kneeling Nun Tuff (Fig. 10) (Hoare et al., 2022; Mandl, 2019). Rindjani represents a low-Ti endmember in the spectrum of magnetite compositions analyzed thus far. A clear relationship emerges when these fractionation factors are plotted against the Ti content of magnetite (Fig. 10), confirming previous observations by Hoare et al. (2022) that magnetite will fractionate Ti isotopes more strongly at any given temperature with increased Ti in the mineral. Our new data allow us to refine the temperature and compositional dependence of the magnetite-melt equilibrium isotopic fractionation, using a weighted linear regression to yield,

$$\Delta^{49}Ti_{magnetite-melt\ (1000K)}\ (‰) = [(-0.058 \pm 0.015)*TiO_2 + (0.15 \pm 0.24)]10^6/T^2 \quad (5)$$

where TiO_2 is the weight percent of TiO_2 in the oxide phase, and T is in kelvin.

Given that the Ti content of magnetite partly determines its Ti isotope mineral-melt fractionation factor, it is important to consider what influences oxide composition in magmatic systems. Unlike many silicates, the Ti content of oxides at any given temperature is not solely a function of the Ti content of the melt. For instance, sample LO-38, which contains the most Ti-rich magnetite of all our mineral separates, crystallized when melt TiO_2 was at its lowest, near the end of the differentiation sequence. Another important control on oxide composition is oxygen fugacity (as indicated by the Fe^{3+}/Fe^{2+} ratio of the melt), which affects Ti partitioning in magnetite through the coupled substitution ($2Fe^{3+} \leftrightarrow Fe^{2+}+Ti^{4+}$), which defines the solid solution between magnetite ($Fe^{2+}Fe^{3+}_2O_4$) and ulvöspinel ($Fe^{2+}_2TiO_4$). Coupled $Fe^{2+}+Ti^{4+}$ substitution into oxides is favored at lower oxygen fugacity when less Fe^{3+} is present (i.e., Sauerzapf et al., 2008), which is consistent with the observation that anhydrous, more reduced magmas produce more Ti-rich magnetite (see Heard Island, Fig. 10) than hydrous, more oxidized magmas (see Santorini, Rindjani, Fig. 10). It is likely that this relationship between Ti isotopic fractionation and oxygen fugacity becomes more complicated when ilmenite is present, because, although ilmenite-bearing melts are generally less oxidized, ilmenite has been found to fractionate Ti isotopes to a lesser degree than titanomagnetite in the same suites (Fig. 9, Hoare et al., 2022). However, for calc-alkaline suites where Fe-Ti oxide crystallization is dominantly magnetite, oxygen fugacity may be a useful predicter of Ti isotopic fractionation, and vice versa.

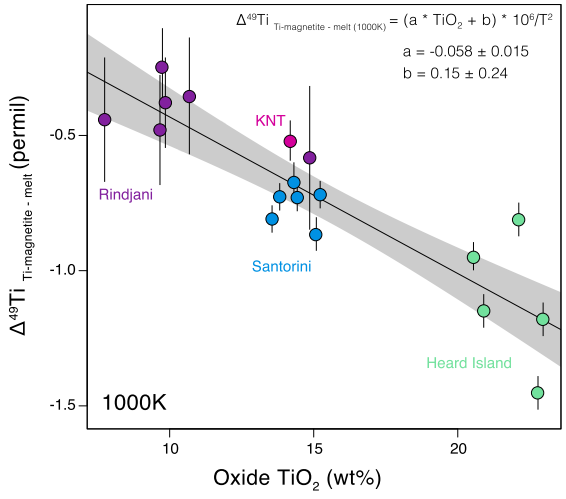

Fig. 10. Titanium isotopic fractionation factor between titanomagnetite-melt at 1000 K as a function of TiO_2 contents in titanomagnetite; uncertainties are 95% CI. Santorini and Heard Island data from Hoare et al. (2022); Kneeling Nun Tuff (rhyolite) data from Mandl (2019).

4.1.3. Melt composition and structure

Another possible cause of variable Ti isotopic fractionation in magmatic systems is the Ti bonding environment in the melt, which is affected by the melt composition. At high temperature, the sole control on Ti isotopic fractionation is the bond strength (Bigeleisen and Mayer, 1947; Urey, 1947; Schauble, 2004; Dauphas et al., 2012). Because the structure of silicate melts is uncertain, one cannot easily apply *ab initio* methods to calculate Ti bond strength and equilibrium fractionation factors in melts. Nevertheless, insights into Ti coordination can be revealed using X-ray Absorption Spectroscopy (XAS), which can inform *ab initio* calculations. Data from XAS analysis of natural and synthetic glasses ranging from basalts to rhyolites reveal that most Ti is in five-fold coordination, but with varying amounts of Ti in four- and six-fold coordination as well (Farges and Brown, 1997). Basalts contain 30–50% of Ti in 6-fold sites, with an average Ti coordination of 5.4, while more felsic melts contain 30–60% of Ti in 4-fold sites with an average Ti coordination of 4.5. This trend suggests that the coordination of Ti in melts is influenced by the degree of melt polymerization, meaning that mineral-melt fractionation factors could increase from mafic to felsic melts as the average coordination number of Ti in the melt decreases and bond strengths increase.

In Fig. 8C, the calculated fractionation factors for Rindjani samples are plotted against whole rock SiO_2 to determine whether Ti isotopic fractionation increases with melt polymerization. There is a slight positive trend with SiO_2, largely because the most evolved sample (LO-38) has the largest fractionation factor. However, this increase in isotopic

fractionation is likely due to the change in oxide composition of LO-38, which has the largest oxide Ti content (Table 2). Even with the increased isotopic fractionation observed in LO-38, a weighted regression of the fractionation factors *vs.* SiO_2 indicates there is no statistically significant relationship between isotopic fractionation and melt polymerization (Fig. 8C).

The abundance of network modifiers (Na, K) that change the structure of the melt may also influence Ti isotopic fractionation. Non-bridging oxygen to tetrahedral cations (NBO/T) and (Na+K)/Ca ratio of the Rindjani lavas are plotted against SiO_2 in Fig. 11, together with the samples studied by Farges and Brown (1997) (open symbols) for their Ti coordination. Despite expectations that changes in major element chemistry would drive changes in Ti coordination of the melt, we see little evidence for that effect, nor is it clearly expressed in Ti isotopes. The calculated NBO/T ratio of Rindjani bulk samples decreases dramatically over the differentiation sequence (similar to other igneous suites, see (Hoare et al., 2020), and network modifiers (Na + K)/Ca steadily increase. However, the most similar samples from Farges and Brown Farges and Brown (1997) indicate average Ti-coordination of 5.5, 5.3, and 5.4 (or $^{[5]}$Ti:$^{[6]}$Ti ratios of 50:50, 70:30, and 60:40, respectively), which may indicate that Ti-coordination does not change very much with changing melt structures. Further work is needed to characterize Ti coordination in representative magma differentiation series to determine whether melt composition exerts any control on Ti isotopic fractionation during magmatic differentiation.

4.2. Fe isotope systematics

Unlike previous studies that have documented Fe isotopic fractionation in magmatic systems (Teng et al., 2008; Schuessler et al., 2009; Sossi et al., 2012; Weyer and Seitz, 2012; Du et al., 2022), we find negligible Fe isotopic fractionation in bulk rocks and mineral separates (Fig. 5). Under equilibrium conditions, iron isotopes can fractionate in magmas due to differences in Fe redox state between melt and crystallizing minerals, as well as different bonding environments between melts and minerals. In both melts and minerals, Fe^{3+} forms stronger bonds than Fe^{2+} (Dauphas et al., 2012; Roskosz et al., 2006), so at equilibrium more Fe^{3+}-rich melts and minerals tend to be enriched in the heavy isotopes of iron relative to more Fe^{2+}-rich phases. The degree of mineral-melt fractionation therefore depends on the contrast in Fe^{3+}/Fe^{2+} between melt and minerals. A complication for iron is the fact that Fe^{2+} in more silicic and more polymerized melts tends to form stronger bonds than Fe^{2+} in more mafic magmas and minerals (Dauphas et al., 2017). Kinetic isotopic fractionation effects associated with diffusion (Teng et al., 2011; Sio et al., 2013; Richter et al., 2009; Oeser et al., 2015) can also induce stable Fe isotopic fractionation in magmatic rocks and minerals.

The absence of Fe isotopic fractionation in the Rindjani lavas and minerals suggests that, due to its more oxidized nature, there is enhanced removal of Fe^{3+} as magnetite that prevents the residual melt from becoming Fe^{3+}-enriched and isotopically heavy. The enhanced Fe^{3+} removal is most likely caused by the crystallization of magnetite, which is estimated in other Rindjani studies to have a Fe^{2+}/Fe^{3+} ratio of 0.88 in basaltic andesites to 0.82 in trachydacites ($Fe^{3+}/Fe_{TOT} \approx 0.55$) (Métrich et al., 2017). Importantly, the lack of ilmenite lowers the removal rate of Fe^{2+} compared to less oxidized differentiation suites; this effect can be seen in Fig. 12A, where the modal abundance of minerals in our samples indicate that magnetite accounts for 40 to 90% of Fe removal. These results are also consistent with the findings of Zhao et al. (2022), who hypothesized that the composition of magnetite controls the direction and magnitude of Fe isotopic fractionation: pure (low-Ti) magnetite enhances removal of Fe^{3+} from the melt, and prevents the melt from evolving to isotopically heavy compositions.

We can also evaluate how the Fe/Mn ratio evolved during magmatic differentiation, because Mn^{2+} has very similar partitioning behavior as Fe^{2+} and Fe/Mn fractionation will reflect the partitioning of Fe^{2+} and Fe^{3+} between melt and minerals. A plot of Fe_2O_3*/MnO ratio (where Fe_2O_3* represents total Fe) *vs.* -ln(f $Fe_{remaining}$)(Fig. 12B) shows a slope of 0 for samples that do not contain magnetite, followed by a decreasing slope in samples that experienced magnetite fractionation, when Fe is more compatible than Mn. The data support a scenario where Fe^{2+} was removed more quickly early in the differentiation, and possibly allowed for Fe isotopic fractionation; however, any isotopic fractionation that occurred was too small to change bulk rock δ^{56}Fe beyond our measured precision, and once magnetite began crystallizing, there was very little isotopic fractionation at all.

To further explore Fe mass balance, the Fe^{2+} *vs.* Fe^{3+} removal rate accomplished by the mineral assemblage is estimated in Fig. 12A, assuming $Fe^{3+}/Fe_{TOT} = 0.55$ for magnetite and 0.05 for clinopyroxene and amphibole. We see that following the appearance of magnetite, Fe^{3+}/Fe_{TOT} of solids range from ~0.3 to 0.5 (Fig. 12C), similar to calculated Fe^{3+}/Fe_{TOT} values of oxidized silicate melts from which those solids are removed (Fig. 12D). Similar Fe^{3+}/Fe_{TOT} values between crystals and melt, as predicted by the calculations, is consistent with the lack of Fe isotopic fractionation observed in the mineral separates. Collectively, these findings suggest that the absence of Fe isotopic fractionation in differentiated calc-alkaline magmas is a consequence of their elevated oxygen fugacity.

4.3. Potential for paired Fe and Ti isotope applications in future studies

Our study provides one of the first demonstrations of the power of pairing Fe and Ti stable isotopic analyses to elucidate the crystallization history of an igneous differentiation suite. Iron stable isotopes have long been recognized to be useful for tracing changes in redox, but the fact that Fe is hosted in and isotopically fractionated by many different

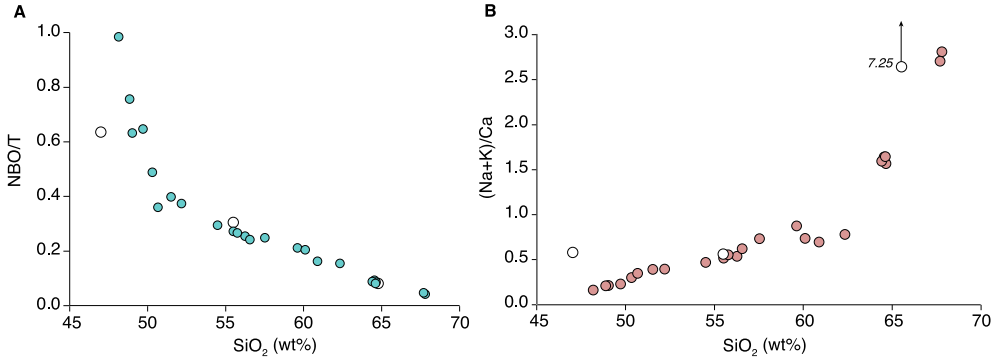

Fig. 11. (A) Calculated NBO/T (nonbridging O/tetragonal O) of bulk rocks plotted against whole rock SiO_2 (wt%). (B) The mole fractions of (Na + K)/Ca in bulk rocks plotted against whole rock SiO_2 (wt%). Open symbols are from Farges and Brown (1997) and include BCR-2 (SiO_2 47.0 wt%, average Ti-coordination 5.5) a synthetic calc-alkaline composition (SiO_2 55.5 wt%, average Ti-coordination 5.3), and a pantellerite (SiO_2 64.8 wt%, average Ti-coordination 5.4).

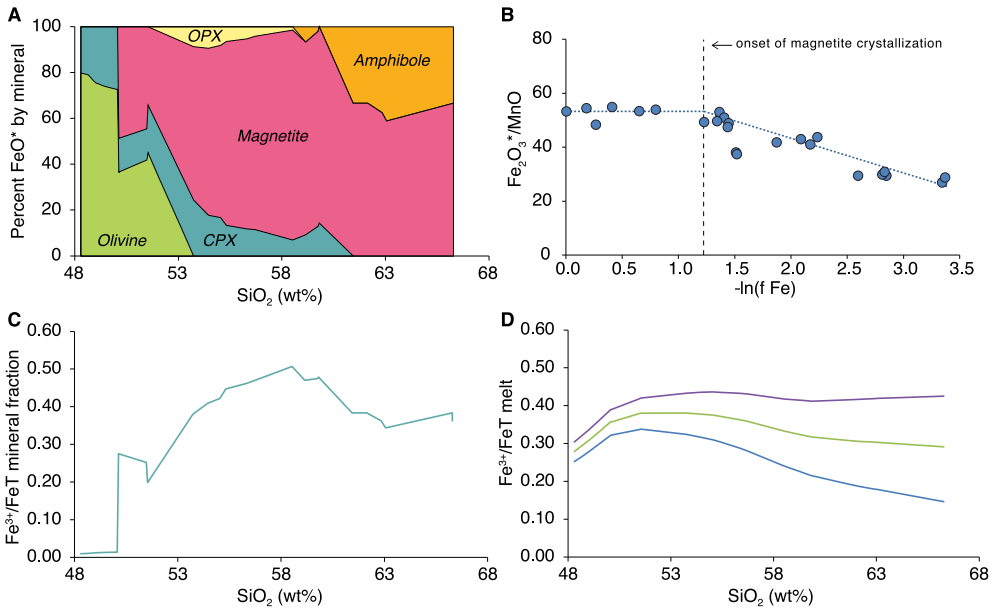

Fig. 12. (A) Calculated percent of total FeO* by mineral, based on modal abundances of whole rock samples and excluding the glass phase. (B) Bulk rock Fe_2O_3*/MnO ratio *vs.* the negative natural log of the fraction of Fe remaining in the melt. Iron is removed more quickly than Mn following the appearance of magnetite as a consequence of increased Fe^{3+} removal. (C) Calculated Fe^{3+}/FeT (total Fe) ratios of crystallizing minerals using the modal abundance of phenocrysts and assuming Fe^{3+}/FeT = 0.55 for magnetite (Métrich et al., 2017), 0.05 for clinopyroxene and amphibole, and 0 for olivine and orthopyroxene (D) Calculated Fe^{3+}/FeT ratios of three silicate melts in response to crystallizing the assemblage of panel C, with starting Fe^{3+}/FeT values of 0.25, 0.28, and 0.30.

minerals has posed a challenge. Iron isotopes in arc volcanic rocks are additionally complicated by the fact that they are sensitive to mantle melting mechanisms (e.g., Foden et al., 2015), mantle heterogeneity (e.g., Williams and Bizimis, 2014), and mobilization by fluids (e.g., Telus et al., 2012). In comparison, Ti resides in fewer phases and is not redox-sensitive in terrestrial settings. Titanium isotopes appear mainly sensitive to fractional crystallization, which often simplifies interpretation. In both individual isotopic systems, it remains difficult to tell the difference between fractional crystallization and remelting/recycling processes.

It was recently discovered that Ti isotopes are indirectly redox-sensitive because they are fractionated by Fe-Ti oxides and the degree of isotopic fractionation can be related to the Fe^{2+}/Fe^{3+} content of the oxides (Hoare et al., 2022). In this study, we extend that relationship to show that oxidized arc magmas such as Rindjani will experience muted Ti isotopic fractionation and little-to-no Fe isotopic fractionation, due to the absence of ilmenite and Ti-rich magnetite that would otherwise induce large isotopic fractionations in both isotope systems. This pairing could be especially useful for igneous rocks that lack the context of a complete differentiation suite or have lost their original tectonic context and the crystallization history is unknown. Such rocks could contain low FeO and TiO_2 abundances, indicating that they experienced crystallization, but paired Fe and Ti isotopes could reveal the mineral assemblage and redox conditions responsible.

5. Conclusions

Titanium isotopic data of bulk lava and mineral separate pairs from Rindjani Volcano, Indonesia, indicate that calc-alkaline magmas show less isotopic fractionation than other magmatic suites due to two compounding factors: (1) The dominant oxide, magnetite, is Ti-poor compared to other suites as a result of lower melt TiO_2 and higher fO_2; consequently, its mineral-melt fractionation factor is smaller than that for Ti-rich magnetite observed in tholeiitic/alkaline series; and (2) While magnetite crystallization is still the dominant phase removing TiO_2 from the melt, removal of non-isotopically-fractionated Ti by silicates becomes increasingly important to consider, and serves to decrease bulk rock Ti isotopic fractionation factor. Iron isotopic data for the same samples are also impacted by Rindjani's oxidized composition and show no isotopic evolution with differentiation. Together, Ti and Fe stable isotopes may reveal important information about mineralogy and redox conditions in differentiated igneous suites and may be a target for future studies.

Declaration of Competing Interest

The authors declare that they have no known competing financial interests or personal relationships that could have appeared to influence the work reported in this paper.

Data Availability

Data are available through Mendeley Data at https://doi.org/10.17632/256nf7z8by.1.

Acknowledgements

This study benefitted from comments by editors Jeff Catalano and Sheng-Ao Liu, reviewer Marc-Alban Millet and two anonymous reviewers. Part of the data reported here were acquired through the senior thesis work of M.T. at UCSB. We thank Allison Greaney for co-supervision of this senior thesis. This work was funded by NSF EAR-PF to Johnson (1952809), NASA grants 80NSSC17K0744 (HW), 000306-002 (HW), 80NSSC21K0380 (EW), 80NSSC20K0821 (EW), NSF grant EAR-2001098 (CSEDI), and funding from DOE to Dauphas, and NSF EAR1757313 to Rudnick. Johnson was additionally supported by NSF EAR-2131643 to Mauricio Ibañez-Mejia.

Appendix A. Supplementary material

Research Data.xlsx description: This file contains all major and trace element data, all Ti and Fe isotopic data, and mineral specific SEM EDS data generated for this study, as well as the original petrographic descriptions for each sample from Toc (2018). Supplementary material to this article can be found online at https://doi.org/10.1016/j.gca.2023.06.016.

References

Aarons, S.M., Reimink, J.R., Greber, N.D., Heard, A.W., Zhang, Z., Dauphas, N., 2020. Titanium isotopes constrain a magmatic transition at the Hadean-Archean boundary in the Acasta Gneiss Complex. Sci. Adv. 6, eabc9959.

Aarons, S.M., Dauphas, N., Blanchard, M., Zeng, H., Nie, N.X., Johnson, A.C., Greber, N. D., Hopp, T., 2021a. Clues from ab initio calculations on titanium isotopic fractionation in tholeiitic and calc-alkaline magma series. ACS Earth Space Chem. 5, 2466–2480.

Aarons, S.M., Johnson, A.C., Rader, S.T., 2021b. Forming Earth's continental crust: A nontraditional stable isotope perspective. Elements 17, 413–418.

Bigeleisen, J., Mayer, M.G., 1947. Calculation of equilibrium constants for isotopic exchange reactions. J. Chem. Phys. 15, 261–267.
Craddock, P.R., Dauphas, N., 2011. Iron isotopic compositions of geological reference materials and chondrites. Geostand. Geoanal. Res. 35, 101–123.
Dauphas, N., Pourmand, A., Teng, F.Z., 2009. Routine isotopic analysis of iron by HR-MC-ICPMS: How precise and how accurate? Chem. Geol. 267, 175–184.
Dauphas, N., Roskosz, M., Alp, E.E., Golden, D.C., Sio, C.K., Tissot, F.L.H., Hu, M.Y., Zhao, J., Gao, L., Morris, R.V., 2012. A general moment NRIXS approach to the determination of equilibrium Fe isotopic fractionation factors: application to goethite and jarosite. Geochim. Cosmochim. Acta. 94, 254–275.
Dauphas, N., John, S.G., Rouxel, O., 2017. Iron isotope systematics. Rev. Mineral. Geochem. 82, 415–510.
Deng, Z., Moynier, F., Sossi, P.A., Chaussidon, M., 2018. Bridging the depleted MORB mantle and the continental crust using titanium isotopes. Geochem. Perspect. Lett. 9, 11–15.
Deng, Z., Chaussidon, M., Savage, P., Robert, F., Pik, R., Moynier, F., 2019. Titanium isotopes as a tracer for the plume or island arc affinity of felsic rocks. PNAS 116, 1132–1135.
Deng, Z., Moynier, F., Villeneuve, J., Jensen, N.K., Liu, D., Cartigny, P., Mikouchi, T., Siebert, J., Agranier, A., Chaussidon, M., Bizzarro, M., 2020. Early oxidation of the martian crust triggered by impacts. Sci. Adv. 6, eabc4941.
Dideriksen, K., Baker, J.A., Stipp, S.L.S., 2006. Iron isotopes in natural carbonate minerals determined by MC-ICP-MS with a 58Fe-54Fe double spike. Geochim. Cosmochim. Acta. 70, 118–132.
Du, D.H., Tang, M., Li, W., Kay, S.M., Wang, X.L., 2022. What drives Fe depletion in calc-alkaline magma differentiation: Insights from Fe isotopes. Geol. 50, 552–556.
Farges, F., Brown Jr, G.E., Rehr, J.J., 1996. Coordination chemistry of Ti (IV) in silicate glasses and melts: I. XAFS study of titanium coordination in oxide model compounds. Geochim. Cosmochim. Acta. 60, 3023–3038.
Farges, F., Brown Jr, G.E., 1997. Coordination chemistry of titanium (IV) in silicate glasses and melts: IV. XANES studies of synthetic and natural volcanic glasses and tektites at ambient temperature and pressure. Geochim. Cosmochim. Acta. 61, 1863–1870.
Foden, J.D., 1983. The petrology of the calcalkaline lavas of Rindjani volcano, east Sunda arc: a model for island arc petrogenesis. J. Petrol. 24, 98–130.
Foden, J., Sossi, P.A., Wawryk, C.M., 2015. Fe isotopes and the contrasting petrogenesis of A-, I-and S-type granite. Lithos 212, 32–44.
Ghiorso, M.S., Gualda, G.A., 2015. An H_2O–CO_2 mixed fluid saturation model compatible with rhyolite-MELTS. Contrib. Mineral. Petrol. 169, 1–30.
Greber, N.D., Dauphas, N., Puchtel, I.S., Hofmann, B.A., Arndt, N.T., 2017a. Titanium stable isotopic variations in chondrites, achondrites and lunar rocks. Geochim. Cosmochim. Acta. 213, 534–552.
Greber, N.D., Dauphas, N., Bekker, A., Ptáček, M.P., Bindeman, I.N., Hofmann, A., 2017b. Titanium isotopic evidence for felsic crust and plate tectonics 3.5 billion years ago. Science 357, 1271–1274.
Greber, N.D., Pettke, T., Vilela, N., Lanari, P., Dauphas, N., 2021. Titanium isotopic compositions of bulk rocks and mineral separates from the Kos magmatic suite: Insights into fractional crystallization and magma mixing processes. Chem. Geol. 578, 120303.
Grove, T.L., Brown, S.M., 2018. Magmatic processes leading to compositional diversity in igneous rocks: Bowen (1928) revisited. Am. J. Sci. 318, 1–28.
Gualda, G.A., Ghiorso, M.S., Lemons, R.V., Carley, T.L., 2012. Rhyolite-MELTS: a modified calibration of MELTS optimized for silica-rich, fluid-bearing magmatic systems. J. Petrol. 53, 875–890.
He, X., Ma, J., Wei, G., Wang, Z., Zhang, L., Zeng, T., Zhang, Z., 2022. Mass-dependent fractionation of titanium stable isotopes during intensive weathering of basalts. Earth Planet. Sci. Lett. 579, 117347.
Heard, A.W., Aarons, S.M., Hofmann, A., He, X., Ireland, T., Bekker, A., Qin, L., Dauphas, N., 2021. Anoxic continental surface weathering recorded by the 2.95 Ga Denny Dalton Paleosol (Pongola Supergroup, South Africa). Geochim. Cosmochim. Acta. 295, 1–23.
Hoare, L., Klaver, M., Saji, N.S., Gillies, J., Parkinson, I.J., Lissenberg, C.J., Millet, M.A., 2020. Melt chemistry and redox conditions control titanium isotope fractionation during magmatic differentiation. Geochim. Cosmochim. Acta. 282, 38–54.
Hoare, L., Klaver, M., Muir, D.D., Klemme, S., Barling, J., Parkinson, I.J., Lissenberg, C.J., Millet, M.A., 2022. Empirical and experimental Constraints on Fe-Ti oxide-melt titanium isotope fractionation factors. Geochim. Cosmochim. Acta. 326, 253–272.
Johnson, A.C., Aarons, S.M., Dauphas, N., Nie, N.X., Zeng, H., Helz, R.T., Romaniello, S. J., Anbar, A.D., 2019. Titanium isotopic fractionation in Kilauea Iki lava lake driven by oxide crystallization. Geochim. Cosmochim. Acta. 264, 180–190.
Klaver, M., MacLennan, S.A., Ibañez-Mejia, M., Tissot, F.L., Vroon, P.Z., Millet, M.A., 2021. Reliability of detrital marine sediments as proxy for continental crust composition: The effects of hydrodynamic sorting on Ti and Zr isotope systematics. Geochim. Cosmochim. Acta. 310, 221–239.
Le Maitre, R.W., Streckeisen, A., Zanettin, B., Le Bas, M.J., Bonin, B., Bateman, P. (Eds.), 2005. Igneous rocks: a classification and glossary of terms: recommendations of the International Union of Geological Sciences Subcommission on the Systematics of Igneous Rocks. Cambridge University Press.
Leitzke, F.P., Fonseca, R.O.C., Göttlicher, J., Steininger, R., Jahn, S., Prescher, C., Lagos, M., 2018. Ti K-edge XANES study on the coordination number and oxidation state of Titanium in pyroxene, olivine, armalcolite, ilmenite, and silicate glass during mare basalt petrogenesis. Contrib. Mineral. Petrol. 173, 1–17.
Mandl, M. B., 2019. Titanium isotope fractionation on the Earth and Moon: Constraints on magmatic processes and Moon formation (Doctoral dissertation, ETH Zurich).
Métrich, N., Vidal, C.M., Komorowski, J.C., Pratomo, I., Michel, A., Kartadinata, N., Prambada, O., Rachmat Surono, H., 2017. New insights into magma differentiation and storage in holocene crustal reservoirs of the lesser sunda arc: The Rinjani-Samalas volcanic complex (Lombok, Indonesia). J. Petrol. 58, 2257–2284.
Millet, M.A., Dauphas, N., 2014. Ultra-precise titanium stable isotope measurements by double-spike high resolution MC-ICP-MS. J. Anal. At. Spectrom. 29, 1444–1458.
Millet, M.A., Dauphas, N., Greber, N.D., Burton, K.W., Dale, C.W., Debret, B., Macpherson, C.G., Nowell, G.M., Williams, H.M., 2016. Titanium stable isotope investigation of magmatic processes on the Earth and Moon. Earth Planet. Sci. Lett. 449, 197–205.
Nazzareni, S., Molin, G., Skogby, H., Dal Negro, A., 2004. Crystal chemistry of Ti3+-Ti4+-bearing synthetic diopsides. Eur. J. Mineral. 16, 443–449.
Nie, N.X., Dauphas, N., Alp, E.E., Zeng, H., Sio, C.K., Hu, J.Y., Chen, X., Aarons, S.M., Zhang, Z., Tian, H.C., Wang, D., 2021. Iron, magnesium, and titanium isotopic fractionations between garnet, ilmenite, fayalite, biotite, and tourmaline: Results from NRIXS, ab initio, and study of mineral separates from the Moosilauke metapelite. Geochim. Cosmochim. Acta. 302, 18–45.
Oeser, M., Dohmen, R., Horn, I., Schuth, S., Weyer, S., 2015. Processes and time scales of magmatic evolution as revealed by Fe–Mg chemical and isotopic zoning in natural olivines. Geochim. Cosmochim. Acta. 154, 130–150.
Richter, F.M., Dauphas, N., Teng, F.Z., 2009. Non-traditional fractionation of non-traditional isotopes: evaporation, chemical diffusion and Soret diffusion. Chem. Geol. 258, 92–103.
Roskosz, M., Luais, B., Watson, H.C., Toplis, M.J., Alexander, C.M.D., Mysen, B.O., 2006. Experimental quantification of the fractionation of Fe isotopes during metal segregation from a silicate melt. Earth Planet. Sci. Lett. 248, 851–867.
Rouxel, O.J., Bekker, A., Edwards, K.J., 2005. Iron isotope constraints on the Archean and Paleoproterozoic ocean redox state. Science 307, 1088–1091.
Rzehak, L.J., Kommescher, S., Kurzweil, F., Sprung, P., Leitzke, F.P., Fonseca, R.O., 2021. The redox dependence of titanium isotope fractionation in synthetic Ti-rich lunar melts. Contrib. Mineral. Petrol. 176, 1–16.
Rzehak, L.J., Sebastian, K., Liam, H., Florian, K., Peter, S., 2022. Redox-dependent Ti stable isotope fractionation on the Moon: implications for current lunar magma ocean models. Contrib. Mineral. Petrol. 177, 1–20.
Saji, N.S., Rudnick, R.L., Gaschnig, R.M., Millet, M.A., 2023. Titanium isotope evidence for the high topography of Nuna and Gondwana-Implications for Earth's redox and biological evolution. Earth Planet. Sci. Lett. 615, 118214.
Sauerzapf, U., Lattard, D., Burchard, M., Engelmann, R., 2008. The titanomagnetite–ilmenite equilibrium: new experimental data and thermo-oxybarometric application to the crystallization of basic to intermediate rocks. J. Petrol. 49, 1161–1185.
Schauble, E.A., 2004. Applying stable isotope fractionation theory to new systems. Rev. Mineral. Geochem. 55, 65–111.
Schuessler, J.A., Schoenberg, R., Sigmarsson, O., 2009. Iron and lithium isotope systematics of the Hekla volcano, Iceland—evidence for Fe isotope fractionation during magma differentiation. Chem. Geol. 258, 78–91.
Sio, C.K.I., Dauphas, N., Teng, F.Z., Chaussidon, M., Helz, R.T., Roskosz, M., 2013. Discerning crystal growth from diffusion profiles in zoned olivine by in situ Mg–Fe isotopic analyses. Geochim. Cosmochim. Acta. 123, 302–321.
Sossi, P.A., Foden, J.D., Halverson, G.P., 2012. Redox-controlled iron isotope fractionation during magmatic differentiation: an example from the Red Hill intrusion, S. Tasmania. Contrib. Mineral. Petrol. 164, 757–772.
Telus, M., Dauphas, N., Moynier, F., Tissot, F.L., Teng, F.Z., Nabelek, P.I., Craddock, P.R., Groat, L.A., 2012. Iron, zinc, magnesium and uranium isotopic fractionation during continental crust differentiation: The tale from migmatites, granitoids, and pegmatites. Geochim. Cosmochim. Acta. 97, 247–265.
Teng, F.Z., Dauphas, N., Helz, R.T., 2008. Iron isotope fractionation during magmatic differentiation in Kilauea Iki lava lake. Science 320, 1620–1622.
Teng, F.Z., Dauphas, N., Helz, R.T., Gao, S., Huang, S., 2011. Diffusion-driven magnesium and iron isotope fractionation in Hawaiian olivine. Earth Planet. Sci. Lett. 308, 317–324.
Urey, H.C., 1947. The thermodynamic properties of isotopic substances. J. Chem. Soc. (Resumed) 562–581.
Vidal, C.M., Métrich, N., Komorowski, J.C., Pratomo, I., Michel, A., Kartadinata, N., Robert, V., Lavigne, F., 2016. The 1257 Samalas eruption (Lombok, Indonesia): the single greatest stratospheric gas release of the Common Era. Sci. Rep. 6, 34868.
Wang, W., Huang, S., Huang, F., Zhao, X., Wu, Z., 2020. Equilibrium inter-mineral titanium isotope fractionation: Implication for high-temperature titanium isotope geochemistry. Geochim. Cosmochim. Acta. 269, 540–553.
Weyer, S., Seitz, H.M., 2012. Coupled lithium-and iron isotope fractionation during magmatic differentiation. Chem. Geol. 294, 42–50.
Weyer, S., Anbar, A.D., Brey, G.P., Münker, C., Mezger, K., Woodland, A.B., 2005. Iron isotope fractionation during planetary differentiation. Earth Planet. Sci. Lett. 240, 251–264.
Whitford, D.J., Foden, J.D., Varne, R., 1978. Sr isotope geochemistry of calcalkaline and alkaline lavas from the Sunda arc in Lombok and Sumbawa, Indonesia. Carnegie Inst. Washington Yearbook 77, 613–619.
Williams, H.M., Bizimis, M., 2014. Iron isotope tracing of mantle heterogeneity within the source regions of oceanic basalts. Earth Planet. Sci. Lett. 404, 396–407.
Zhang, J., Dauphas, N., Davis, A.M., Pourmand, A., 2011. A new method for MC-ICPMS measurement of titanium isotopic composition: Identification of correlated isotope anomalies in meteorites. J. Anal. At. Spectrom. 26, 2197–2205.
Zhao, X., Tang, S., Li, J., Wang, H., Helz, R., Marsh, B., Zhu, X., Zhang, H., 2020. Titanium isotopic fractionation during magmatic differentiation. Contrib. Mineral. Petrol. 175, 1–16.
Zhao, J., Wang, X.J., Chen, L.H., Hanyu, T., Shi, J.H., Liu, X.W., Kawabata, H., Xie, L.W., 2022. The effect of Fe–Ti oxide separation on iron isotopic fractionation during basalt differentiation. Contrib. Mineral. Petrol. 177, 1–15.